International Journal of GEOMATE, Sep., 2025 Vol.29, Issue 133, pp.89-96
ISSN: 2186-2982 (P), 2186-2990 (O), Japan, DOI: https://doi.org/10.21660/2025.133.5030
Geotechnique, Construction Materials and Environment

EFFECT OF SUPPLEMENTARY REINFORCEMENT ON FLEXURAL STRENGTH OF REINFORCED CONCRETE BEAMS

*Dang-Bao Tran

Institute of Architecture, Construction and Transportation Training, Thu Dau Mot University, Vietnam

*Corresponding Author, Received: 26 April 2025, Revised: 02 July 2025, Accepted: 06 July 2025

ABSTRACT: This study investigates the flexural behavior of reinforced concrete (RC) beams, modeled using a nonlinear deformation-based fiber method, in accordance with Vietnamese Standard TCVN 5574:2018. The analysis focuses on the effect of supplementary longitudinal reinforcement added to satisfy the code's vertical spacing requirement. The fiber method enables accurate simulation of reinforcement distribution and material nonlinearity across arbitrary cross-sections. Three typical RC beam types-rectangular, T-shaped, and I-shaped-were analyzed under varying reinforcement strategies. The results show that, beyond ensuring serviceability, supplementary reinforcement can significantly enhance structural capacity. Specifically, for the representative reinforcement layouts examined in the case studies, the maximum observed increases in ultimate moment capacity reached 47.74% for rectangular beams, up to 20.36% for T-shaped beams, and nearly 64% for I-shaped beams. This finding demonstrates that a detailing constraint originally intended for crack control can be reframed as a strength optimization opportunity. Although developed under TCVN 5574:2018, the numerical method is essentially code-independent, requiring only idealized stress-strain input and thus applicable to standards such as Eurocode 2 and ACI 318. This adaptability supports broader adoption of performance-based structural design.

Keywords: TCVN 5574:2018, Flexural capacity, Longitudinal reinforcement, Vertical spacing, Nonlinear fiber method, RC beams

1. INTRODUCTION

In RC beams, the maximum spacing between longitudinal reinforcement bars is prescribed in design standards to limit cracking along the side faces. This provision is outlined in several major codes of practice [1-3]. Eurocode 2 [1] stipulates that in beams with an overall depth greater than 600 mm, supplementary reinforcement must be provided along the side faces at a spacing not exceeding 300 mm. Similarly, ACI 318 [2] mandates side-face reinforcement for nonprestressed and select prestressed beams deeper than 914 mm. The required spacing is determined based on the service-level bar stress and the clear cover from the tension face to the nearest flexural reinforcement. Notably, ACI permits these bars to contribute to flexural capacity, provided that strain compatibility is ensured. In addition, TCVN 5574:2018 [3] sets a vertical spacing limit between layers of longitudinal reinforcement to enhance serviceability; the distance between adjacent layers must not exceed the lesser of 400 mm or 1.5 times the section height.

Although these provisions [1-3] are primarily intended to enhance serviceability, the structural contribution of the associated supplementary reinforcement-particularly in terms of flexural capacity-has not been systematically evaluated and remains insufficiently addressed in both design codes and technical literature. This creates a fundamental design contradiction: reinforcement detailing requirements imposed for serviceability may unintentionally improve structural strength, yet this potential benefit is rarely quantified or integrated into design models. To resolve this design contradiction, a deformation-based modeling approach is essential. Unlike deformation-based approaches, traditional force-based methods do not derive internal stresses from actual strain distributions. Instead, they rely on assumed stress blocks and predefined material limits-such as concrete crushing strain and reinforcement yield strength-that vary by national codes, without explicitly modeling the nonlinear stress-strain behavior of materials. As a result, they offer limited ability to capture how reinforcement layout influences internal stress development and strain redistribution, and they are less capable of addressing complex cross-sectional geometries or flexural behavior under biaxial bending.

Although TCVN 5574:2018 permits the use of nonlinear deformation models in structural analysis, prior Vietnamese studies [4-13] have predominantly relied on simplified analytical approaches. These methods are generally suitable for rectangular sections with regular reinforcement layouts, but are inadequate for capturing complex stress redistribution in more irregular configurations. The use of advanced numerical methods-particularly the fiber method [14-18], which is widely recognized for its versatility and precision in analyzing nonlinear behavior across arbitrary cross-sections-remains limited. Consequently, the application of nonlinear

deformation analysis under TCVN 5574:2018 is still underdeveloped, leaving a methodological gap in the current literature.

This study aims to bridge that gap by employing the fiber method to perform nonlinear flexural analysis of RC beams with rectangular, T-shaped, and I-shaped cross-sections, using material models as defined in TCVN 5574:2018. While rooted in the Vietnamese standard, the methodology is computationally adaptable to international design codes, through the substitution of relevant stress-strain relationships. This adaptability supports international relevance and reflects current trends in performance-based structural design.

The objectives of this study are twofold:

(i) To establish a deformation-based computational framework for accurately evaluating the ultimate flexural capacity of RC beams under TCVN 5574:2018;

(ii) To investigate the structural contribution of supplementary longitudinal reinforcement-whether required by vertical spacing criteria or strategically introduced-in the dual context of serviceability compliance and structural optimization.

The structure of this paper is as follows: Section 2 discusses the research significance and context. Section 3 presents the stress-strain models for concrete and reinforcement in accordance with TCVN 5574:2018. Section 4 details the numerical methodology, including fiber discretization and nonlinear deformation analysis. Section 5 illustrates three case studies involving rectangular, T-shaped, and I-shaped RC beams, examining the influence of supplementary reinforcement on flexural capacity. Section 6 concludes with key findings.

2. RESEARCH SIGNIFICANCE

Although vertical reinforcement spacing rules are intended for serviceability, their structural implications-especially from supplementary bars added solely to meet spacing limits-remain underexplored. This study applies a nonlinear, deformation-based numerical method [14-18] to evaluate their flexural contribution. The findings reveal that such bars can enhance strength, supporting more integrated and performance-based reinforcement strategies. While the analysis is based on TCVN 5574:2018 [3], the modeling approach itself is code-independent-requiring only stress-strain input-and can be readily adapted for use with standards such as Eurocode 2 [1] or ACI 318 [2].

3. STRESS–STRAIN DIAGRAMS FOR CONCRETE AND REINFORCING STEEL

To streamline the sectional analysis, this study adopted idealized bilinear stress–strain models defined in TCVN 5574:2018 [3] for concrete in compression and reinforcement in both tension and compression. The tensile strength of concrete was neglected, and a perfect bond between materials was assumed. As illustrated in Fig. 1, these simplifications were introduced to isolate the effects of reinforcement distribution rather than to capture detailed material behavior.

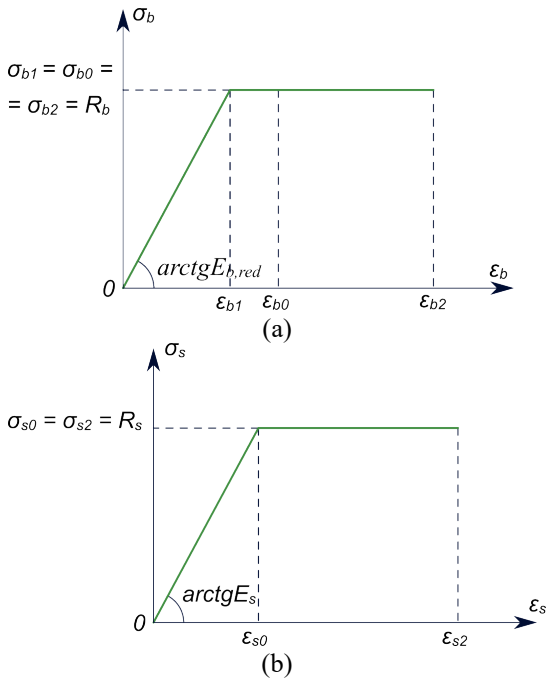

Fig.1 Stress–strain relationships of concrete (a) and reinforcement (b) employed in this study.

The stress–strain behavior of concrete is represented using a bilinear model, mathematically expressed as follows:

$$\begin{cases} \sigma_b = E_{b,red}\varepsilon_b \text{ when } 0 \le \varepsilon_b < \varepsilon_{b1} \\ \sigma_b = R_b \text{ when } \varepsilon_{b1} \le \varepsilon_b \le \varepsilon_{b2} \end{cases}, \quad (1)$$

where σ_b, ε_b represent the compressive stress and strain in the concrete, respectively, and the reduced modulus of elasticity is defined as:

$$E_{b,red} = \frac{R_b}{\varepsilon_{b1,red}}, \quad (2)$$

in which R_b is the design compressive strength of concrete

The relative strain values $\varepsilon_{b1,red}, \varepsilon_{b0}, \varepsilon_{b2}$ are determined in accordance with Clause 6.1.3.2 of [3].

Similarly, the stress–strain behavior of reinforcing steel is modeled using a bilinear relationship:

$$\begin{cases} \sigma_s = \varepsilon_s E_s \text{ when } 0 \le \varepsilon_s < \varepsilon_{s0} \\ \sigma_s = R_s \text{ when } \varepsilon_{s0} \le \varepsilon_s \le \varepsilon_{s2} \end{cases}, \quad (3)$$

where σ_s, ε_s denote the stress and strain in the reinforcement, respectively, while E_s represents its is

the modulus of elasticity of the reinforcement. The ultimate tensile strain is taken as ε_{s2} = 0.025. Accordingly, the yield strain is determined as follows

$$\varepsilon_{s0} = \frac{R_s}{E_s}. \quad (4)$$

4. FIBER DISCRETIZATION AND NUMERICAL INTEGRATION METHOD

Figure 2 illustrates the fiber discretization technique applied to RC cross-sections under combined bending and axial compression. This method, widely used in nonlinear section analysis [14-18], involves subdividing the cross-section into numerous small elements (fibers), each characterized by its area, material properties, and location.

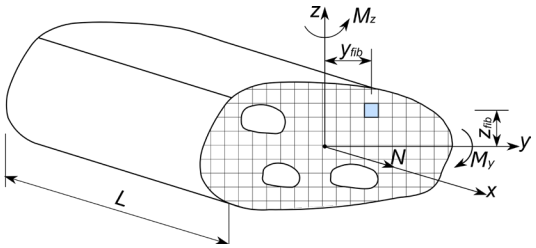

Fig. 2 Fiber discretization technique applied to RC cross-sections under combined bending and axial compression

To evaluate the internal force vector and sectional stiffness matrix, numerical integration is performed over the discretized section. Among available methods, this study adopts the rectangular (midpoint) integration due to its simplicity and proven accuracy, especially in handling discontinuous stress and stiffness distributions [17, 18]. It should be noted that the focus of this study is not to compare the effectiveness of numerical integration schemes.

Assuming the section remains plane after deformation (Bernoulli's hypothesis), the deformation state is fully described by the axial strain ε_x and curvatures κ_y and κ_z. The strain at each fiber is then computed based on its relative position with respect to the centroidal axis of the transformed section, which ensures strain compatibility across the entire cross-section.

The sectional stiffness matrix is determined by integrating the contribution of each fiber, considering both material stiffness and fiber location. The continuous and discrete forms are expressed as:

$$\boldsymbol{k_s} = \int_A E_t \begin{bmatrix} 1 & z & -y \\ z & z^2 & -yz \\ -y & -yz & y^2 \end{bmatrix} dA \approx \sum_{i=1}^{N_{fib}} E_{ti} \begin{bmatrix} 1 & z_i & -y_i \\ z_i & z_i^2 & -y_i z_i \\ -y_i & -y_i z_i & z_i^2 \end{bmatrix} A_i, \quad (5)$$

where E_t represents the modulus derived from the material's stress-strain relationship

A_i is the area of each fiber in the cross-section

(y_i, z_i) are coordinates relative to the centroidal axis of the transformed section

N_{fib} denotes the total number of discretized fibers used for numerical integration

The internal force vector is computed by integrating the normal stresses in each fiber, weighted by their area and location:

$$\boldsymbol{s} = \begin{Bmatrix} N \\ M_y \\ M_z \end{Bmatrix} = \int_A \begin{pmatrix} 1 \\ z \\ -y \end{pmatrix} dA \approx \sum_{i-1}^{N_{fib}} \begin{pmatrix} 1 \\ z_i \\ -y_i \end{pmatrix} \sigma_i A_i \quad (6)$$

in which σ is the normal stress

This leads to the nonlinear sectional equilibrium equation:

$$\boldsymbol{k_s}.\boldsymbol{u} = \boldsymbol{s}, \quad (7)$$

where $\boldsymbol{u} = \{\varepsilon_x, \kappa_y, \kappa_z\}^T$ is the generalized deformation vector.

The nonlinear problem is solved iteratively by enforcing equilibrium between the external load vector $\boldsymbol{s_{ext}}$ and the internal response:

$$\boldsymbol{R} = \boldsymbol{s_{ext}} - \boldsymbol{s}, \quad (8)$$

where $\boldsymbol{R}$ is the residual force vector, quantifying the imbalance at the sectional level.

To solve the nonlinear equilibrium condition, the Newton-Raphson method is adopted. The iterative procedure follows these steps:

1. **Initialization**: Assign initial values for $\boldsymbol{u} = \{\varepsilon_x, \kappa_y, \kappa_z\}$
2. **Strain Computation:** Calculate fiber strains with respect to the centroidal axis of the transformed section, assuming plane section behavior
3. **Stress Evaluation:** Use nonlinear material models to compute fiber stresses σ_i
4. Assemble $\boldsymbol{k_s}$ and **s** via rectangular integration
5. **Compute Residual**
6. **Convergence Check**:
   - If $\|\boldsymbol{R}\| < 10^{-5}$, converged
   - If the ultimate compressive strain in the concrete or the ultimate tensile strain in the reinforcement is reached
7. **Update**: Solve for $\Delta\boldsymbol{u}$ via
   $$\boldsymbol{k_s}.\Delta\boldsymbol{u} = \boldsymbol{R}, \quad (9)$$
   then update: $\boldsymbol{u} \leftarrow \boldsymbol{u} + \Delta\boldsymbol{u}$, and repeat the process.

5. VERIFICATION EXAMPLES

The following examples illustrate the influence of supplementary mid-depth reinforcement on ultimate flexural capacity. All models were analyzed using a fiber-based nonlinear method in MATLAB R2015a.

Although coarse meshes may yield sufficient accuracy [17], each cross-section was discretized into 400 fibers to avoid concerns over sensitivity. Mesh convergence analysis was not pursued, as it lies beyond the study's scope.

5.1 Example 1

A rectangular beam with a 300 × 500 mm cross-section is evaluated under bottom fiber tension, with a 30 mm concrete cover.

The material properties are specified as follows:

Concrete B15, with an elastic modulus $E_c = 24.3 \times 10^3$ MPa, and a design compressive strength $R_b = 8.5$ MPa;

CB300V reinforcing steel, with an elastic modulus $E_s = 2 \times 10^5$ MPa, and a design yield strength R_s=260 MPa.

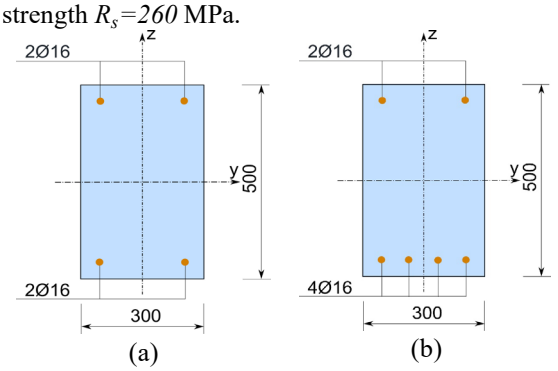

Fig. 3 Cross-section of the rectangular section used in Example 5.1

In the configuration with symmetric reinforcement placed at both the top and bottom (Fig. 3a), the analytical method estimated the ultimate moment capacity to be 44.32 kNm. In comparison, the nonlinear fiber model predicted a slightly higher value of 46.5 kNm, corresponding to a deviation of 4.92%.

For the configuration where the reinforcement is concentrated primarily in the tension zone (Fig. 3b), the analytical method calculated an ultimate moment of 90.37 kNm, while the nonlinear fiber model produced a closely matching result of 91.1 kNm, with a minimal difference of just 0.81%.

Table 1 demonstrates the increase in ultimate moment capacity due to the addition of supplementary reinforcement, consisting of two bars with diameters ranging from 2Ø10 to 2Ø16. For the symmetric configuration, the ultimate moment increased from 55.3 kN·m to 68.7 kNm, corresponding to a 47.74% improvement over the baseline value of 46.5 kNm. In the tension-dominant configuration, the capacity improved from 99.5 kNm to 110.9 kNm, representing a 21.73% increase relative to the baseline of 91.1 kNm.

In all symmetric configurations with supplementary bars ranging from 2Ø10 to 2Ø16, yielding consistently occurs at the ultimate load. Figure 4 presents a representative example of this behavior, illustrating the reinforcement stress distribution for two configurations-a top-bottom symmetric layout and a tension-dominant configuration-both incorporating 2Ø16 supplementary bars at mid-heigh.

Table 2 shows the variation in neutral axis depth, measured from the extreme compression fiber, for different cases with and without supplementary reinforcement. It can be observed that the compression zone height increases with the inclusion of supplementary bars. Overall, the data from the tables and figures in this example confirm that supplementary reinforcement effectively improves the flexural capacity of the beam in all configurations, with top-bottom symmetric placement generally yielding greater enhancement than tension-focused arrangements.

Table 1. Ultimate moment capacities-rectangular section with supplementary reinforcement (kNm)

Configuration	2Ø10	2Ø12	2Ø14	2Ø16
Symmetric	55.3	59	63.5	68.7
Tension-Dominant	99.5	102.5	106.6	110.9

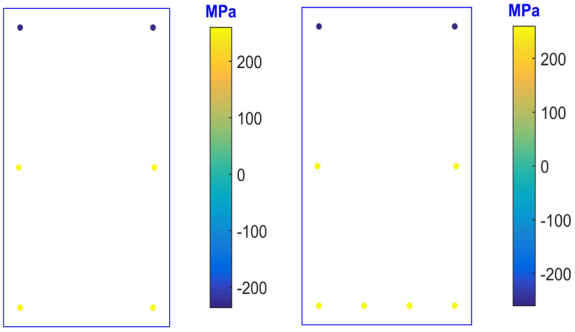

Fig. 4 Reinforcement stress distribution with 2Ø16 supplementary bars at ultimate moment: (a) symmetric; (b) tension-focused.

Table 2. Neutral axis Depth (mm) for various reinforcement configurations with and without supplementary reinforcement

Configuration	Without	2Ø10	2Ø12	2Ø14	2Ø16
Symmetric	42	48	50	52	58
Tension-Dominant	57	73	80	97	104

5.2 Example 2

A T-shaped RC beam is analyzed under bending, with tension occurring at the bottom fiber and a concrete cover of 30 mm. The material properties are specified as follows:

Concrete B15, with an elastic modulus $E_c = 24.3 \times 10^3$ MPa, and a design compressive strength $R_b = 8.5$ MPa;

CB400V reinforcing steel, with an elastic modulus $E_s = 2 \times 10^5$ MPa, and a design yield strength R_s=350 MPa.

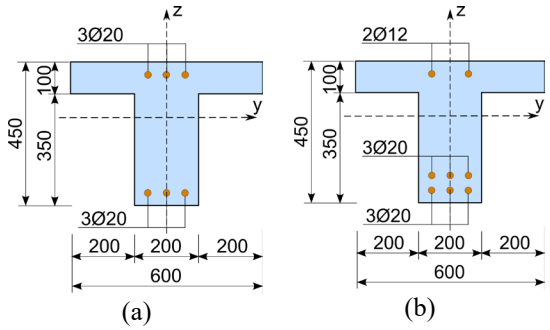

Fig. 5 Cross-section of the T section beam used in Example 5.2

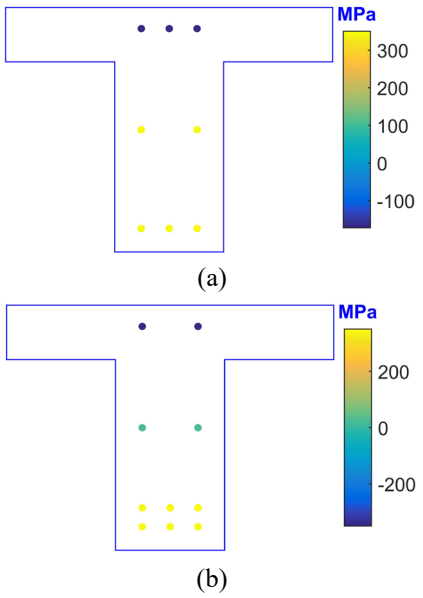

Fig. 6 Reinforcement stress distribution with 2Ø12 supplementary bars at ultimate moment: (a) symmetric; (b) tension-focused.

In the top-bottom symmetric reinforcement layout (Fig. 5a), the analytical method predicted an ultimate moment capacity of 121.98 kNm, while the nonlinear fiber method yielded 126.7 kNm-a difference of 3.87%. For the tension-focused configuration (Fig. 5b), the analytical result was 219.2 kN·m, and the fiber method yielded 221.6 kN·m, with a difference of 1.09%.

Table 3 demonstrates the increase in ultimate moment capacity resulting from the addition of supplementary reinforcement. Notably, the supplementary bars used in this example are not mandatory under the provisions of [3]. In the symmetric configuration (with reinforcement placed equally at the top and bottom), increasing the supplementary bars from 2Ø10 to 2Ø16 raises the ultimate moment from 137.1 kNm to 152.5 kNm, representing a 20.36% improvement over the baseline. In contrast, under the tension-concentrated configuration, the same increase in bar size results in only a slight rise in ultimate moment-from 223.1 kNm to 224.1 kNm-indicating a marginal gain relative to the baseline.

Table 3. Ultimate moment capacities for T section in example 5.2 (kNm)

Configuration	2Ø10	2Ø12	2Ø14	2Ø16
Symmetric	137.1	141.5	146.5	152.5
Tension-Dominant	223.1	223.5	223.8	224.1

Table 4 Stress in the supplementary reinforcement for both configurations at ultimate moment (MPa)

Configuration	2Ø10	2Ø12	2Ø14	2Ø16
Symmetric	350	350	350	350
Tension-Dominant	126.8	113.1	98.5	29

Table 5. Neutral axis depth (mm) for different reinforcement configurations and supplementary reinforcement

Configuration	Without	2Ø10	2Ø12	2Ø14	2Ø16
Symmetric	50	55	56	60	61
Tension-Dominant	176	190	194	197	200

Figure 6 illustrates the reinforcement stress distribution at the ultimate bending moment for two configurations: a top-bottom symmetric layout and a tension-dominant configuration, both incorporating 2Ø12 supplementary bars at mid-height. Table 4 summarizes the stress values in the supplementary bars across multiple reinforcement configurations at the ultimate moment. It is observed that in the symmetric case, the supplementary bars yield under the ultimate load, whereas in the tension-focused configuration, they remain elastic, indicating limited utilization. This contrast can be attributed to the neutral axis location: as shown in Table 5, it remains within the flange in the symmetric layout, but shifts into the web in the tension-dominant case due to the

concentration of reinforcement in the tension zone.

5.3 Example 3

An I-shaped RC beam, illustrated in Fig. 7, is analyzed with a concrete cover of 40 mm. The beam is subjected to flexural loading, with tensile stresses concentrated along the bottom fiber, and the coordinate system is positioned at the centroid of the section. The material properties used in the analysis include concrete grade B15, with a design compressive strength of 8.5 MPa, and CB400V reinforcing steel, with a design yield strength of 350 MPa.

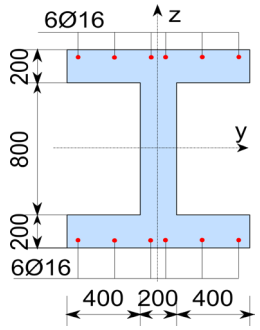

Fig. 7 Baseline reinforcement configuration without supplementary bars in Example 5.3

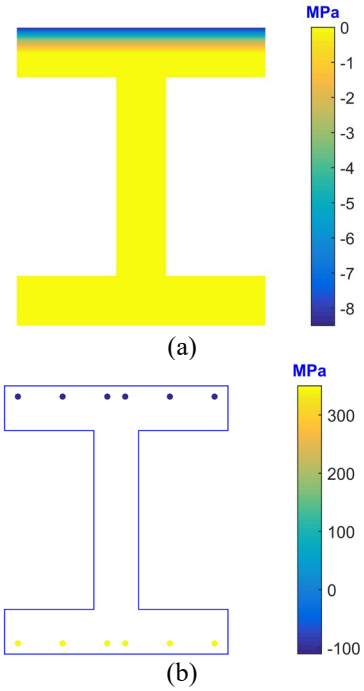

Fig. 8 Stress distribution in the concrete and reinforcement at the ultimate bending moment with I cross-section in Fig. 7

This case highlights the inherent limitations of conventional internal force-based design methods, especially when dealing with irregular geometries. TCVN 5574:2018 does not provide explicit guidance for I-shaped sections. In contrast, the nonlinear fiber method, which accounts for the actual reinforcement layout and full cross-sectional geometry, yields an ultimate moment capacity of 478 kNm , with a corresponding neutral axis depth of 54 mm measured from the extreme compression fiber. This result underscores the critical role of advanced numerical modeling in accurately assessing the structural performance of complex cross-sections. The stress distribution at the ultimate moment state is shown in Fig. 8.

To further evaluate the influence of supplementary longitudinal reinforcement, three configurations are considered, each differing in quantity and vertical distribution of added bars. These supplementary bars are placed along the web, between the main tension and compression reinforcements, to either comply with or deliberately exceed the 450 mm vertical spacing limit specified by TCVN 5574:2018.

The alternative layouts are defined as follows (with vertical positions measured from the section centroid):

- Layout 1: Two bars at mid-depth violating the vertical spacing limit
- Layout 2: Four bars placed at two levels ($z = \pm 108$ mm) and symmetrically distributed at $y = \pm 52$ mm along the flange width
- Layout 3**:** Eight bars distributed across four levels ($z = \pm 108$ mm, and ± 324 mm), symmetrically distributed at $y = \pm 52$ mm along the flange width.

Table 6. Ultimate moment capacities and neutral axis depths with 2 supplementary bars at mid-depth

Configuration	2Ø10	2Ø12	2Ø14	2Ø16
Moment [kNm]	510.1	521.5	540	556
Neutral Axis Depth [mm]	57	58	60	63

Table 7. Ultimate moment capacities and neutral axis depths with 4 supplementary bars at $z = \pm 108$ mm and ± 52 mm

Configuration	4Ø10	4Ø12	4Ø14	4Ø16
Moment [kNm]	538.5	566.3	596.7	633.1
Neutral Axis Depth [mm]	61	65	68	73

Table 8. ultimate moment capacities and neutral axis depths with 8 supplementary bars at $z = \pm 52, \pm 108, \pm 324$ mm

Configuration	8Ø10	8Ø12	8Ø14	8Ø16
Moment [kNm]	599.2	652.5	715.5	783.5
Neutral Axis Depth [mm]	67	75	84	98

The results of the nonlinear fiber analysis are summarized in Tables 6-8, showing the ultimate moment capacities and corresponding variations in neutral axis depth (measured from the extreme compression fiber) for different supplementary reinforcement configurations. For each configuration, the influence of increasing the bar diameter from Ø10 to Ø16 is also reported.

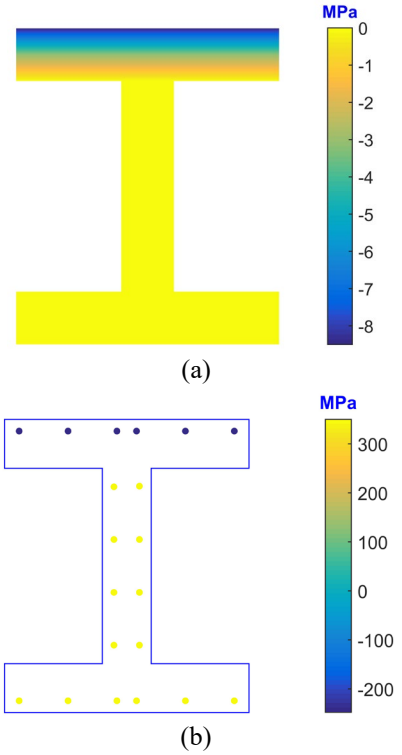

Fig. 9 Stress distribution in concrete and reinforcement at the ultimate bending moment for the I-shaped cross-section with eight supplementary bars.

The results clearly show that supplementary reinforcement, regardless of compliance with the vertical spacing limit, consistently enhances flexural capacity compared to the baseline value of 478 kNm (see Table 6). Notably, increasing the number of bars and distributing them vertically across the section height further amplifies this effect, reaching up to 783.5 kNm with 8Ø16 bars.

Fig. 9 presents the stress distribution in concrete and reinforcement at the ultimate bending moment for the I-shaped section with eight supplementary bars, providing insight into the internal stress state. The compressive stress at the top fiber reaches its maximum value, corresponding to the ultimate concrete strain of 0.0035. Meanwhile, the tensile stress in the bottom reinforcement and all supplementary bars reaches the design yield strength. The compressive stress in the reinforcement reaches-247.6 MPa.

This suggests a deeper design insight: although the spacing limit is imposed for serviceability (e.g., crack control), it indirectly creates an opportunity for structural improvement. Supplementary bars, when strategically placed-even beyond code requirements-can be leveraged to improve material efficiency and flexural resistance.

This example also reinforces the necessity of deformation-based modeling in capturing the nonlinear response of complex cross-sections, such as I-beams, which are not addressed directly in TCVN 5574:2018. The positive contradiction here-between serviceability-driven constraints and strength optimization-can be resolved through refined computational approaches like the fiber method.

6. CONCLUSION

This study employed the nonlinear fiber method, using material models defined in TCVN 5574:2018, to evaluate the flexural performance of RC beams with rectangular, T-shaped, and I-shaped cross-sections. Particular attention was given to supplementary longitudinal reinforcement, either required to meet the vertical spacing limit or optionally introduced to explore its structural benefit.

The results confirm that reinforcement initially added to satisfy serviceability requirements can also contribute to an increase in ultimate moment capacity. The extent of this enhancement depends on the arrangement of compression and tension reinforcement. In the analyzed examples, the maximum observed increases reached 47.74% in rectangular beams, 20.36% in T-shaped beams, and nearly 64% in I-shaped beams.

From a practical design perspective, these gains-ranging from 20% to over 60%- can allow for more economical use of reinforcement for the same load-bearing capacity, leading to reduced steel consumption. This implies not only material cost savings but also potential reductions in embodied carbon (CO_2) associated with steel production.

These findings carry meaningful implications for design practice. First, the vertical spacing provision in TCVN 5574:2018-originally intended for crack control-can be reframed as a structural optimization opportunity when analyzed using nonlinear fiber method. Second, the nonlinear fiber method enables more accurate assessment of reinforcement strategies, especially in members with irregular geometry or complex reinforcement layouts where simplified approaches may be inadequate.

Lastly, while the analysis is based on TCVN 5574:2018 [3], the modeling approach itself is code-independent, requiring only stress-strain input, and can be readily adapted to design standards such as

Eurocode 2 [1] or ACI 318 [2]. This supports a broader shift toward performance-based design grounded in nonlinear material response and realistic sectional behavior.

It should be noted that this study did not examine the sensitivity of results to mesh density, numerical integration schemes, or convergence criteria (e.g., tolerances of 10^{-3} vs. 10^{-5}). Shear-related effects were also not considered. These aspects are acknowledged as limitations and are recommended for further investigation in future studies.

7. REFERENCES

[1] EN 1992-1-1:2023. Design of Concrete Structures - Part 1-1: General Rules and Rules for Buildings, European Committee for Standardization (CEN), Brussels, 2023, pp 01-402.

[2] ACI Committee 318. Building Code Requirements for Structural Concrete (ACI 318-19) and Commentary. American Concrete Institute, Farmington Hills, MI, 2019. pp 01-529.

[3] Ministry of Science and Technology. TCVN 5574:2018 – Design of Concrete and Reinforced Concrete Structures, Vietnam, 2018, pp.01–194. (in Vietnamese)

[4] Lê, M.L. (2017). Some updates in the draft of TCVN 5574:2017. Journal of Construction Science and Technology), pp. 55-61. (in Vietnamese

[5] Bá, N.N. (2019). Limits of reinforcement ratio in flexural RC structures according to TCVN 5574:2018. Journal of Construction Science and Technology, Vol.1, pp.22-28. (in Vietnamese)

[6] Vo, T.L. (2019). Flexural section analysis of RC beams based on deformation. Journal of Science and Technique – Section on Special Construction Engineering, Vol.2(2), pp. 88-96. (in Vietnamese)

[7] Tuấn, T. (2020). Flexural behavior of RC beams through moment–curvature diagrams under TCVN 5574:2018. Journal of Construction Science and Technology, pp.62-69. (in Vietnamese)

[8] Linh, N.N., Tân, N.N., Quang, N.V., & Minh, P.Q. (2020). Theoretical and experimental study on the ultimate moment of RC beams using the nonlinear deformation model. Vietnam Journal of Science and Technology – Part B, Vol.62(1), pp. 36-41. (in Vietnamese)

[9] Long, T.N., Phúc, P.V., & Hà, N.T. (2020). Analysis of skew bending in RC beams using nonlinear model. Journal of Construction Science and Technology, pp.23-35. (in Vietnamese)

[10] Nguyen, T.D., Pham, V.A., & Tran-Thi, K.H. (2022, November). Investigating the ultimate bending strength of reinforced concrete section under different non-linear constitutive models according to the design standard TCVN 5574–2018. In Proc. 7th National Scientific Conference on Applying New Technology in Green Buildings (ATiGB), IEEE, pp.150-155.

[11] Cao, V.T., & Trương, M.P. (2023). Flexural behavior of rectangular RC beams using nonlinear material model. Journal of Construction, pp.110-115. (in Vietnamese)

[12] Thi, T. V. T., Thi, B. Q. V., & Gridnev, S. Y. (2024). Analysis of reinforced concrete double-cantilever beams in road-bridge superstructures using nonlinear deformation model. International Journal of GEOMATE, 26(116), pp. 93-101.

[13] Van-Phuc, P., Ngoc-Long, T., Trong-Ha, N., & Duy-Thuan, P. (2021). An Analysis of the Stress-Strain State of Reinforced Concrete Beam Cross-Sections Subjected to Biaxial Bending. International Journal of GEOMATE, 21(84), pp. 9-23.

[14] Sadeghian, V., & Vecchio, F. (2018). The modified compression field theory: then and now. ACI Structural Journal, SP-328, 3–1.

[15] Spacone, E., Filippou, F.C., & Taucer, F.F. (1996). Fibre beam–column model for non‐linear analysis of RC frames: Part I. Formulation. Earthquake Engineering & Structural Dynamics, 25(7), pp.711–725.

[16] Spacone, E., Filippou, F.C., & Taucer, F.F. (1996). Fibre beam–column model for non‐linear analysis of RC frames: Part II. Applications. Earthquake Engineering & Structural Dynamics, 25(7), pp.727–742.

[17] Kostic, S.M., & Filippou, F.C. (2012). Section discretization of fiber beam-column elements for cyclic inelastic response. Journal of Structural Engineering, 138(5), pp.592–601.

[18] Kostic, S. M., & Filippou, F. C. (2023). An adaptive section discretization scheme for the nonlinear dynamic analysis of steel frames. Journal of Structural Engineering, 149(4), 04023015.